

Under the Hood of Membership Inference Attacks on Aggregate Location Time-Series

Apostolos Pyrgelis*
EPFL
apostolos.pyrgelis@epfl.ch

Carmela Troncoso
EPFL
carmela.troncoso@epfl.ch

Emiliano De Cristofaro
UCL & Alan Turing Institute
e.decristofaro@ucl.ac.uk

Abstract

Aggregate location statistics are used in a number of mobility analytics to express how many people are in a certain location at a given time (but not who). However, prior work has shown that an adversary with some prior knowledge of a victim’s mobility patterns can mount membership inference attacks to determine whether or not that user contributed to the aggregates. In this paper, we set to understand why such inferences are successful and what can be done to mitigate them. We conduct an in-depth feature analysis, finding that the volume of data contributed and the regularity and particularity of mobility patterns play a crucial role in the attack. We then use these insights to adapt defenses proposed in the location privacy literature to the aggregate setting, and evaluate their privacy-utility trade-offs for common mobility analytics. We show that, while there is no silver bullet that enables arbitrary analysis, there are defenses that provide reasonable utility for particular tasks while reducing the extent of the inference.

1 Introduction

The increasing availability of location data enables a growing number of mobility applications, ranging from forecasting events [18] to monitoring depressive states [7], etc. Some of these tasks often rely on aggregates: rather than single users’ trajectories, these express the number of people transiting in some geographic areas, or points of interest. For instance, Waze builds traffic models using average driving speeds [51], while Uber provides aggregate data for urban planning purposes [48]. Also, Telefonica monetizes footfall statistics through advertising and business analytics [45].

Evidently, mobility patterns expose sensitive attributes, e.g., lifestyles, religious inclinations, etc. as well as users’ home and work place, which can be used to de-anonymize them [13]. These concerns do not effectively lessen when data is aggregated; in fact, mobility profiles [36] or trajectories [52] can still be inferred. In [37], Pyrgelis et al. show that, given an aggregate time-series, an adversary can launch a *membership inference attack* (MIA), inferring whether or not a target user contributed to those aggregates. They also evaluate the effectiveness of differentially private mechanisms to thwart the attack, showing that they successfully mitigate inference but at the cost of a dramatic reduction in utility.

However, previous research has not provided meaningful explanations as to what makes membership inference possible, e.g., what spatio-temporal factors contribute to the attack’s success and in what contexts, nor which users are most vulnerable and why. This lack of understanding also hampers the design of defenses geared to provide acceptable privacy-utility trade-offs. In this paper, we aim to address this gap by (1) carrying out an in-depth feature analysis to gain an understanding of the reasons behind the attack’s success, and (2) using the insights provided by the analysis to inform the design of defense strategies and evaluate their privacy-vs-utility trade-off. For both tasks, we use two real-world mobility datasets capturing different mobility patterns, namely, the Transport For London (TFL) and the San Francisco Cabs (SFC) datasets.

Understanding MIAs’ success. We follow a dimensionality reduction approach to shed light on the spatio-temporal factors that are important for the inference. We use Principal Component Analysis (PCA) [22] on the aggregate location data and examine the correlation coefficients in the components. We discover that PCA not only helps with the analysis but, as spatio-temporal correlations prevail in the aggregates, also *significantly* boosts MIA’s performance. We also study the importance of features (e.g., number of events, number of unique locations visited etc.) in a classifier trained on users’ mobility characteristics and identify the factors that help the inference. Among other things, we find that the amount of data contributed to the aggregation plays an important role, that movements in less popular places/times can reveal a user’s presence in the aggregates, and that the attack’s success is linked to the uniqueness and regularity of mobility.

Defenses. We then evaluate the effectiveness of location privacy defense strategies, configured using insights from the feature analysis, at mitigating the inferences. For each defense, we measure the gain in privacy as well as various utility metrics relevant to mobility analytics performed on aggregate locations, such as forecasting, hotspot discovery, location labeling, and anomaly detection. Our analysis demonstrates that, while there is no single approach that enables arbitrary tasks with high levels of privacy, there are strategies that can efficiently balance the privacy-utility trade-off for specific spatio-temporal tasks. For instance, data generalization can be used for forecasting and map inference, suppression techniques allow ranking hotspots, while sampling yields good results on sparser datasets, especially for data analysis based on the distribution over the locations. Furthermore, perturbation de-

*Work done in part while the author was at UCL.

fenses that guarantee differential privacy enable hotspot discovery, while other tasks, e.g., anomaly detection, can be performed only when less noise is injected.

Contributions. In summary, we make several contributions:

1. We present a novel approach for MIA on aggregate location time-series using PCA, which substantially improves the performance of the attack while removing the need for costly feature extraction.
2. Using two datasets representative of different users’ mobility patterns, we gain a deep understanding of the mobility characteristics that make users vulnerable to the attack, and identify the spatio-temporal features determining the success of MIAs vis-à-vis different priors.
3. We study the effectiveness of location privacy defenses against MIA showing that for some settings they can provide protection while retaining utility for particular analytics tasks.

2 Preliminaries

2.1 Datasets

We perform experiments on two mobility datasets which have often been used in location privacy research [42, 36, 37]. Together, they capture very different mobility patterns, generated from public transport commuters and taxis, respectively.

Transport For London (TFL). This dataset includes 60M trips made by 4M passengers on the TFL transportation network, between Monday, March 1st and Sunday, March 28th, 2010, using their “Oyster” travel cards. For each trip, we have the oyster id (hashed with salt), start time, tap-in station id, end time, and tap-out station id. Trips are made over 582 tube and overground stations, or *Regions of Interests (ROIs)*. We sample the dataset and retain the data of the 10K oyster ids with the largest amount of trips. We set the time granularity to 1 hour and, for each oyster id, we generate a binary matrix whose rows indicate ROIs and columns indicate timeslots. Each element is 1 if the user tapped-in or out at a certain station, at a certain time, and 0 otherwise. When a passenger does not tap in or out of any station within a given timeslot, we assign it to a special ROI, denoted as *null*. Overall, the sampled dataset contains a total of 7.3M events, with the 10K oysters reporting an average of 728 ± 16 total tap-in/tap-out events, over 20 ± 9 unique ROIs, and it is relatively sparse as the oysters are in the transportation system, on average, for 115 ± 21 out of the 672 hourly slots (28 days).

San Francisco Cabs (SFC). The SFC dataset contains mobility trajectories of taxis in the San Francisco area between May 17 and June 10, 2008 [34]. Each record includes a cab identifier, latitude, longitude, and a timestamp. Overall, we have 11M GPS coordinates generated by 536 taxis. We retain 3 weeks of data (Monday, May 19 to Sunday, June 8), keeping only traces within an area of 30.3mi^2 to cover downtown San Francisco. We split this area in a uniform grid of 10×10 , with cells (ROIs) of 0.3mi^2 each, and we set the time granularity to 1 hour. Again, for each cab we generate a binary matrix (with rows representing ROIs and columns timeslots),

Symbol	Description
Adv, Ch	Adversary, Challenger
\mathcal{P}	Adversarial Prior Knowledge
\mathcal{U}	Set of Mobile Users
\mathcal{S}	Set of Locations (ROIs)
\mathcal{T}	Time Period Considered
$\mathcal{T}_O, \mathcal{T}_I$	Observation and Inference Periods
m	Aggregation Group Size
α	Percentage of Users Whose Locations are Known (Subset of Locations Prior)
β	Number of Groups Whose Aggregates are Known During \mathcal{T}_O (Participation in Past Groups Priors)

Table 1: Membership Inference Attack Notation.

indicating whether or not a cab transited through a location, at a certain time, and we assign a cab not generating any event within a timeslot to the *null* ROI. Overall, the final dataset contains 2M events generated by 534 cabs, each reporting on average $3,827 \pm 1,069$ events over 78 ± 6 unique ROIs; thus, this dataset is much less sparse than TFL, as taxis report ROIs for 340 ± 94 out of the 504 time slots (21 days).

Aggregates. For both datasets, we compute the aggregate location time-series over a group of users (i.e., passengers or cabs) by adding their binary matrices. The resulting aggregate location time-series indicates the number of users that transit through the TFL and SFC ROIs, over time.

2.2 MIA on Aggregate Location Time-Series

Pyrgelis et al. [37] model membership inference attacks (MIAs) on aggregate locations as a distinguishability game between an adversary (Adv) and a challenger (Ch): Adv needs to distinguish location aggregates, provided by Ch, that include the data of a target user from those that do not. The game has several parameters, including the universe of users \mathcal{U} , the size of the aggregation groups m , and the inference period \mathcal{T}_I during which Adv is being challenged. To mount the attack, Adv uses a classifier trained on data over an observation period \mathcal{T}_O available as part of her “prior knowledge”.

Priors. We consider different types of prior knowledge [37]:

1. **Subset of Locations:** Adv knows the actual locations for a subset of users, including her target. The size of the subset is controlled by a parameter α .
2. **Participation in Past Groups:** Adv knows her target’s participation in aggregates observed during \mathcal{T}_O , with a parameter β indicating the number of groups whose aggregates are known. More precisely, we have:
 - (2a) **Same Groups As Released:** Ch challenges Adv with aggregates computed on the same groups as her prior knowledge;
 - (2b) **Different Groups Than Released:** Adv is challenged on dynamic groups, which should make the inference harder.

To ease presentation, notation is summarized in Table 1.

Privacy Loss. We measure the classifier’s Area Under the Curve (AUC) score, capturing its performance in the distinguishing task for various classification thresholds, and compute the *privacy loss* as the adversarial improvement over a random guess baseline (i.e., AUC score of 0.5).

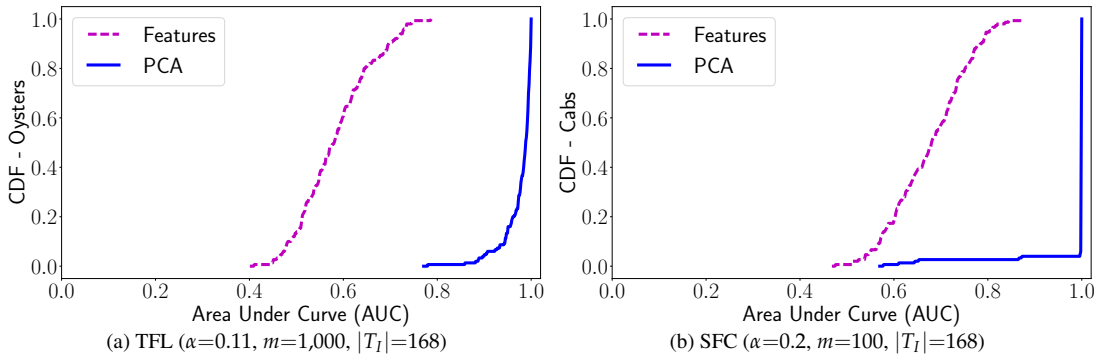


Figure 1: MIA’s performance with Subset of Locations Prior: Features vs. PCA.

3 Understanding Membership Inference on Aggregate Location Time-Series

In this section, we study *what* makes the presence of a user’s location data points in aggregates inferable, and *how* this varies based on the adversary’s prior knowledge.

3.1 Experimental Setup

As done in [37], we split users into three mobility groups (*highly, somewhat, and barely* mobile) and run MIA against 150 users, 50 from each group, sampled at random. To target a user, we create balanced datasets containing aggregate location time-series that include and exclude her location data to train/test the classifier used as a distinguisher by the adversary.

PCA Optimization. The classifier in [37] uses as features simple statistics computed for each location time-series (mean, median, maximum, minimum, variance, standard deviation, and sum). In a first feature analysis we find that, in both TFL and SFC datasets, the variance of the location counts over time is the dominant feature. We then use Principal Components Analysis (PCA) to reduce the dimensionality of the problem and extract valuable information.¹ We feed the components to a Logistic Regression (LR) classifier—we choose LR as it yields the best performance. The use of PCA not only helps us to understand the effects of mobility patterns on MIA, but also *boosts the attack’s performance while also removing the need for costly feature extraction*.

To illustrate this improvement, in Figure 1, we plot the CDF of the classifier’s AUC scores, computed over the 150 target users, for both the feature extraction approach [37] and the dimensionality reduction one when using the **Subset of Locations** prior. The increase on the mean AUC score amounts to 65% for TFL, and 46% for SFC. We observe the same trend, though somewhat less prominently, for the other priors: with **Same Groups As Released**, the improvement is 22% for TFL and 16% for SFC; with **Different Groups Than Released**, it increases by 26% and 17%, respectively.

Roadmap. First, we examine the correlation coefficients within the PCA components, highlighting which spatial and temporal points contribute to the inference. We then train a

machine learning classifier on the mobility characteristics of the victims that are most and least prone to the attack, and investigate its features’ importance to identify factors making the attack more powerful. Specifically, we compute the following statistics of the users’ trajectories: total events (i.e., location-time tuples), unique locations visited, active timeslots, mean locations per timeslot, mean events and active timeslots during week days and weekends, spatial and temporal entropy, and unicity. The latter captures how unique is a user’s travel pattern, as $unicity_u = \sum_{t \in \mathcal{T}} \mathbb{1}^t(u) / |\mathcal{T}|$, where $\mathbb{1}^t(u)$ indicates whether the ordered sequence of locations visited by user u at time t is unique or not.

We also test intuitive hypotheses about the success of MIAs on aggregate locations. For instance, does the volume of data a user contributes to the aggregation affect her susceptibility to the attack? Do users’ movements in less popular locations/times give membership away? Do very unique or very regular mobility patterns increase the attack’s performance?

3.2 Subset of Locations Prior

We first study the case where Adv knows the actual locations for a subset of users during the inference period.

Parameters. We set the percentage of users for which locations are known as $\alpha=0.11$ and $\alpha=0.2$ for TFL and SFC, respectively, and consider the maximum user group size that the adversary can attack: $m=1,000$ for TFL and $m=100$ for SFC. In both cases, the first week is the observation and inference period (i.e., $|T_I|=168$ hourly timeslots), and we create datasets of 2K samples to train and test the classifier (with a 80%–20% train/test split).

3.2.1 TFL

Correlation Coefficients. In Figure 2a, we plot the aggregate correlation coefficients for spatio-temporal points over the 2 most important principal components of each victim. Events in various locations and times yield high correlation values (dark red), i.e., *diverse events contribute to membership inference*. We also find that different stations exhibit different levels of correlation (possibly due to their location, e.g., central vs. residential ones). As for time, we see differences between the patterns of week days (ids 1–120) and of weekends (121–168), with *commuting hours having high correlation values*. Interestingly, for some ROIs, busy mid-day hours also yield high correlation. The same happens with weekend events (right side

¹PCA converts observations of correlated variables to linearly uncorrelated ones (principal components) via an orthogonal transformation. The first principal component accounts for as much variability in the data as possible, and each succeeding one has the largest variance possible while being orthogonal to the previous components [22].

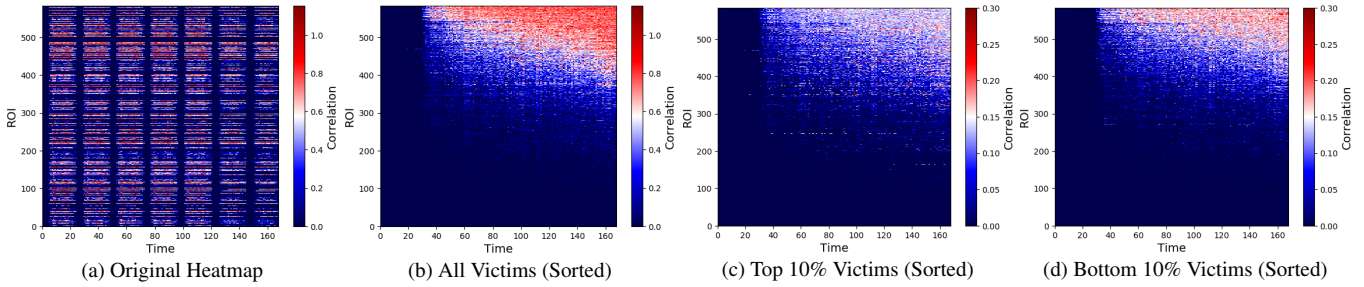


Figure 2: Subset of Locations Prior, TFL ($\alpha=0.11$, $m=1,000$, $|\mathcal{T}_{\mathcal{I}}|=168$). Aggregate spatio-temporal correlation over the top-2 components per victim; heatmap sorted (ascending-order) by location and timeslot popularity computed on (b) all victims, (c) top 10%, and (d) bottom 10% of distinguishable victims.

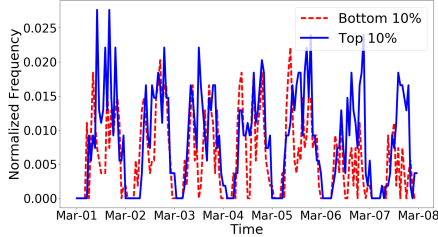


Figure 3: Subset of Locations Prior, TFL ($\alpha=0.11$, $m=1,000$, $|\mathcal{T}_{\mathcal{I}}|=168$). Normalized timeslot frequency over $\mathcal{T}_{\mathcal{I}}$.

of the heatmap): users’ presence in the aggregates might be revealed if they travel at times when the transportation system is less crowded.

Location/Timeslot Popularity. In Figure 2b, we sort the aggregate correlation heatmap, both locations and time, according to their frequency of appearance in the dataset. As expected, the *more popular locations/timeslots yield the highest correlation* (upper-right corner), since most of the events are generated in such locations/times. Nonetheless, data points in popular locations but reported in less popular timeslots (upper-left corner) are also important, suggesting that *commuters can be distinguished in the aggregates if they visit such locations at non-busy times*. Finally, a few points in less popular locations (and various times) are also important for the classifier, i.e., *movements in sparse locations/times can give away a commuter’s presence in the aggregates*.

Susceptibility to MIA. We analyze the susceptibility to MIA of the most and least distinguishable victims. For the top distinguishable victims (Figure 2c), we find very high coefficients for relatively unpopular locations and times (middle part of the heatmap), i.e., *people visiting rare locations at rare times are easy to attack*. The most popular places and times (top right) do yield high correlation, but they do not seem to be as crucial. For the less distinguishable commuters (Figure 2d), popular locations and times (top right part of the heatmap) are the most important, and no other location seems to help the attack. We believe that these are commuters that mostly travel at popular stations/times and their data hides better along with those of the crowd.

To verify these hypotheses we study the aggregate (normalized) frequency of the timeslots in the inference week over the two groups in Figure 3. The distinguishable commuters (blue line) have higher frequency in mid and late evening hours of week days (when the transportation system is less crowded)

Feature	TFL	SFC	Feature	TFL	SFC
Total events	0.03	0.17	Events/weekday	0.01	0.07
Unique locations	0.39	0.01	Events/weekend	0.13	0.03
Active timeslots	0.06	0.23	Spatial entropy	0.01	0.03
Locations per timeslot	0.05	0.30	Temporal entropy	0.06	0.01
Active timeslots/weekday	0.01	0.01	Unicity	0.16	0.17
Active timeslots/weekend	0.11	0.01			

Table 2: Subset of Locations Prior. Feature importance for a Random Forest classifier separating top/bottom 10% distinguishable victims: TFL ($\alpha=0.11$, $m=1,000$, $|\mathcal{T}_{\mathcal{I}}|=168$) and SFC ($\alpha=0.2$, $m=100$, $|\mathcal{T}_{\mathcal{I}}|=168$).

and during weekends; i.e., *sporadic movements at these hours facilitate membership inference*. The less distinguishable oysters (red line) mostly move during “commuting” hours and their privacy is less harmed by the release of aggregates.

Next, we feed the mobility characteristics of the top and bottom 10% distinguishable oysters to a Random Forest classifier and examine which features can separate the two groups (see Table 2). The most important feature is the number of unique locations visited by a user: *visiting more (unique) locations increases the attack’s surface and thus its success*. Second in importance is the unicity, highlighting a link between MIA and the uniqueness of mobility patterns: top victims have a unique mobility pattern for 14 ± 5 timeslots of $\mathcal{T}_{\mathcal{I}}$, while the bottom ones are unique only for 4 ± 1 .

3.2.2 SFC

Correlation Coefficients. In Figure 4a, we plot the aggregate spatio-temporal correlation coefficients, computed over the cabs’ top 5 components. As opposed to TFL, *a large number of locations yield high coefficients, highlighting that GPS movements offer a larger attack surface than tap-in/out events at London stations*. We see a similar effect for time, with *high correlations in mid-day hours*, but also during weekends when fewer drivers are working.

Location/Timeslot Popularity. Unsurprisingly, we find that the most popular locations have high correlation values; see Figure 4b. However, contrary to TFL where only a small subset of stations and times are relevant (recall Figure 2b), in SFC also mid-popular locations (i.e., ids 40-60), as well as certain hours in less popular ROIs (ids 20-40), obtain significant correlation. This suggests that popularity is not as important as in TFL, *there are many regions and times that help membership inference*.

Susceptibility to MIA. We compare the coefficients of the top

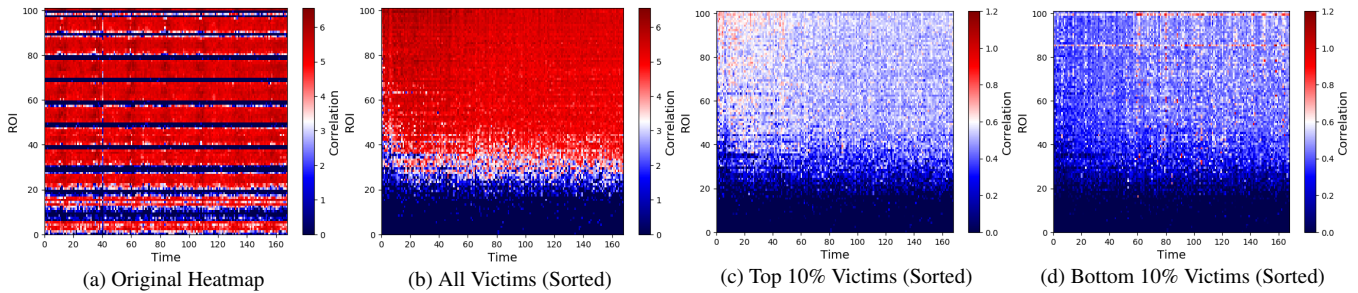


Figure 4: Subset of Locations Prior, SFC ($\alpha=0.2$, $m=100$, $|\mathcal{T}_{\mathcal{I}}|=168$). Aggregate spatio-temporal correlation over the top-5 components per victim: (a) original heatmap; ascending-order sorted heatmap by location and timeslot popularity computed on (b) all victims, (c) top 10%, and (d) bottom 10% of distinguishable victims.

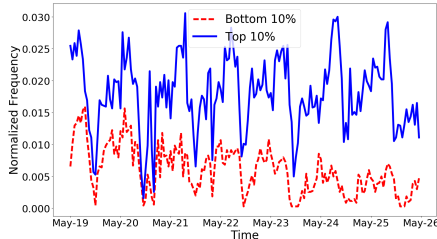


Figure 5: Subset of Locations Prior, SFC ($\alpha=0.2$, $m=100$, $|\mathcal{T}_{\mathcal{I}}|=168$). Normalized timeslot frequency over $\mathcal{T}_{\mathcal{I}}$.

and bottom distinguishable cabs (Figures 4c–4d). The former yield slightly higher coefficients in the most popular locations but during the least busy times. This confirms that *movements in less popular times enhance membership inference*. For these cabs, the counts of popular locations and timeslots also yield high correlation values, i.e., they contribute a large portion of points during the inference week. The heatmap of the least distinguishable cabs is much sparser: most cabs contribute little data and the attack has little information to build on. Similarly to TFL, the most popular locations and timeslots, where most cabs contribute to anyway, yield the highest correlation, i.e., popular regions are not very revealing.

In terms of normalized frequency, Figure 5 shows that the top distinguishable cabs (blue line) have higher frequencies in late night hours of weekdays and during weekends, i.e., *movements in low activity hours facilitate attacks*. Whereas, the less distinguishable cabs (red line) contribute some data at the beginning of the week, but less afterwards. This confirms that the most distinguishable cabs are those which contribute larger volume of spatio-temporal points, i.e., *bigger data contribution enhances MIA performance*.

As for TFL, we study which features are important to separate effectively the top and bottom 10% distinguishable cabs (see Table 2). The top feature is the mean number of locations per timeslot, showing that unlike in TFL where most commuters report similar volumes of data, in the SFC dataset *vehicles with more data points are overall more susceptible to MIAs*. We also observe that, similarly to TFL, MIA’s performance is strongly linked to the uniqueness of cabs’ mobility trajectories. The top distinguishable cabs exhibit larger unicity (their patterns are unique for 124 ± 6 out of the 168 timeslots) than the bottom ones (unique pattern for 38 ± 30 timeslots).

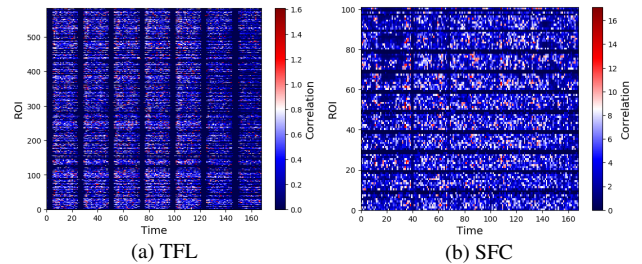


Figure 6: Same Groups As Released Prior. Aggregate spatio-temporal correlation over the top components per victim for (a) TFL ($\beta=500$, $m=9,500$, $|\mathcal{T}_{\mathcal{I}}|=168$) and (b) SFC ($\beta=800$, $m=500$, $|\mathcal{T}_{\mathcal{I}}|=168$).

3.3 Participation In Past Groups Prior

Next, we analyse the case where Adv knows the target victim’s participation in aggregate locations released during an observation period $\mathcal{T}_{\mathcal{O}}$. We consider two settings for this prior: (a) one where the Adv performs inference on the same groups as in the observation period, and (b) another where the inference is made on different groups.

Parameters. We set the size of the groups to $m=9,500$ for TFL and $m=500$ for SFC. We consider $\mathcal{T}_{\mathcal{O}}$ to be the first weeks of each dataset, and use them to construct the prior knowledge the adversary relies on to train her classifier. The attack is run on the last week ($|\mathcal{T}_{\mathcal{I}}|=168$). We configure the number of known groups as $\beta=500$ and $\beta=800$, for TFL and SFC, creating large enough training/testing datasets (of 2K (2.4K) samples for TFL (SFC)).

3.3.1 Same Groups As Released

Correlation Coefficients. We start with the setting where Adv performs MIA on the same groups as those on which she trained her classifier. We plot the aggregate correlation coefficients for the most important principal components of the victims in TFL (top 1 component/victim) and SFC (top 5 components/victim) in Figure 6. For TFL, the most correlated data points now occur during the morning commuting hours of weekdays, highlighting that *regularity in mobility patterns, e.g., the daily commute to work, helps MIA*. This explains the MIA’s great success on TFL with this type of prior [37]. Interestingly, we also find that popular locations/times as well as less popular locations on popular times (and vice versa) contribute to the inference, showing that commuters exhibit different regular patterns that are equally useful for the attack.

For SFC, movements in some weekdays’ slots yield high correlation, i.e., there are some regular cabs that are more susceptible to MIA than others. Looking at the location and timeslot popularity, we find high correlations scattered in the spatio-temporal space. Nonetheless, we observe that movements during less popular timeslots obtain slightly higher correlation values in the components, i.e., cabs regular at such times are prone to MIA. Overall, *the attack does not work very well with this prior when victims do not exhibit the same mobility patterns over the weeks*, as most cabs in SFC.

As for mobility characteristics, we do not analyze them for TFL since all commuters are harmed equally. For SFC, the insights are similar to those for the Different Groups Than Released prior, discussed next.

3.3.2 Different Groups Than Released

Correlation Coefficients. We investigate the setting where Adv performs MIA over different groups than those on which she trained her classifier. Overall, the insights are similar as for the *Same Groups As Released* prior for both datasets (thus, we omit the corresponding heatmaps): regular mobility patterns contribute to the success of MIA. Nevertheless, it is not clear *what* locations or times are more important, i.e., various types of regular patterns make MIA successful.

Susceptibility to MIA. We compare the mobility characteristics of the top and bottom 10% distinguishable victims using a Logistic Regression classifier. Table 3 reports the model’s coefficients for each feature (negative and positive coefficients indicate, resp., the more and less distinguishable victims). For both datasets, the strongest feature for the top victims is the uniqueness of mobility patterns: *the more unique movements are, the easier it is to infer membership on dynamic groups*. With TFL, we find that the top victims have unique pattern for 47 ± 13 out of the 672 hourly timeslots, while the bottom ones exhibit unicity for 32 ± 7 timeslots. With SFC, top victims exhibit unique mobility for 357 ± 45 out of the 504 timeslots, and the bottom ones are unique for 287 ± 85 timeslots.

Features related to time patterns also play an important role in separating the two groups for TFL; e.g., the top distinguishable users are mostly contributing events during days of the week, the bottom ones in the weekends. The results also suggest that top users are mostly regular weekday commuters in less popular ROIs (and thus more unique), while bottom ones travel to locations outside their “regular” pattern during weekends. This is confirmed by other features with high coefficients, e.g., the number of unique locations and spatial entropy. For SFC, the amount of data contributed yields stronger features for the more distinguishable cabs, i.e., ‘regular’ cabs reporting larger volumes of data are more identifiable. For the least distinguishable cabs, the number of unique locations is stronger. Overall, this confirms that when the adversary trains on past groups, *showing up in many locations, but without repeating patterns, can reduce her power*.

3.4 Take Aways

Our analysis provides several interesting conclusions. First of all, we show that the performance of MIA on aggregate lo-

Feature	TFL	SFC	Feature	TFL	SFC
Total events	0.20	-0.36	Events/weekday	-0.47	-0.38
Unique locations	0.78	1.29	Events/weekend	0.64	-0.17
Active timeslots	-0.17	0.05	Spatial entropy	0.52	-0.18
Locations per timeslot	0.01	-0.33	Temporal entropy	0.17	-0.06
Active timeslots/weekday	-0.48	0.28	Unicity	-1.55	-0.68
Active timeslots/weekend	0.42	-0.46			

Table 3: Different Groups Than Released Prior. Model coefficients of a Logistic Regression classifier separating top/bottom 10% distinguishable victims: TFL ($\beta=500, m=9,500, |\mathcal{T}_I|=168$) and SFC ($\beta=800, m=500, |\mathcal{T}_I|=168$).

cation time-series can be significantly boosted using dimensionality reduction techniques such as PCA (up to 65% mean AUC increase for TFL and 46% for SFC), as aggregate location data retains strong spatio-temporal correlations from the data provided by individual users. We also find the spatio-temporal correlations within the principal components to be aligned with the mobility patterns in the data. For instance, commuting patterns emerge quite clearly in the components of the TFL dataset, while dense GPS trajectories create a large attack surface to be exploited in SFC. In both cases, there is a variety of spatio-temporal points and trends that contribute towards to the inference’s success. Thus, designing generic, robust defenses is inevitably an extremely challenging task.

Also, our analysis of the mobility characteristics that best split the most and least distinguishable victims sheds light on which factors affect the success of the inference. We find that: 1) Users who contribute more data points to the aggregation are more susceptible to MIA; 2) Movements in sparse locations/timeslots can give away one’s presence in the aggregates; and 3) Unique and regular mobility patterns are more identifiable in the aggregates.

Finally, we identify factors that *negatively* affect the attack’s performance; e.g., presence in popular locations and times generally limits inferences, and so do irregular movements that do not hold over time when prior knowledge is built using information from the past.

4 Defenses

In this section, we experimentally evaluate how existing strategies commonly used to protect location privacy – configured based on the insights from the analysis presented above – perform in the setting of aggregate location time-series.

4.1 Preliminaries

Experimental Setup. We focus on the cases where MIA works best, to simulate a *worst case scenario* for the defenses. For TFL, we consider the **Same Groups As Released** prior knowledge, with $\beta=500$, groups of $m=9,500$ users, and \mathcal{T}_O being the first 3 weeks of the dataset and \mathcal{T}_I the last one. For SFC, we choose the **Subset of Locations** prior, with $\alpha=0.5$, $m=250$, and both \mathcal{T}_O and \mathcal{T}_I being the first week. We also consider a strategic adversary that knows the mechanism employed by the defender and can use this to optimize her training (i.e., the adversary trains on aggregates perturbed using that defense strategy).

Privacy Gain (PG) Metric. Following Pyrgelis et al. [37], we measure the effectiveness of the defenses as the normalized decrease in the adversarial performance:

$$PG = \begin{cases} \frac{AUC_A - AUC_{A'}}{AUC_A - 0.5} & \text{if } AUC_A > AUC_{A'} \geq 0.5 \\ 0 & \text{otherwise} \end{cases} \quad (1)$$

where AUC_A is the performance on raw aggregates, and $AUC_{A'}$ is the performance of the attack *after* a defense has been applied. PG is a value between 0 and 1, capturing how much the inference power drops towards the random guess baseline (AUC score of 0.5) where users have *perfect* privacy.

4.2 Experimental Evaluation

Our feature analysis shows that, in general, it is not possible to identify a fundamental set of features that, if protected, would deter MIAs for all users. As a result, there is no straightforward approach to distill a defense that directly tackles the core of the problem. Therefore, we explore a range of defenses commonly used in the location privacy literature, namely, generalization, hiding, and perturbation. In the rest of this section, we discuss possible configurations for each strategy to operate in the aggregate location setting. We also report boxplots of the privacy gain (over the users that we attack) for the most interesting defenses configurations in Figures 7a for TFL and 7b for SFC.

4.2.1 Generalization

With generalization, one reduces the precision with which spatio-temporal events are reported [14, 25], and thus their uniqueness [9]. Bucketing techniques, i.e., reporting data in ranges rather than releasing exact statistics, can also be used to this end. This approach has been used to protect privacy in domains such as website fingerprinting, by obfuscating the length of network packets [6]; or social network privacy, by providing inexact statistics to advertisers [49].

Spatial Generalization (SPG). We first experiment varying the spatial granularity, while keeping the temporal resolution to one hour. This technique has been used to decrease the uniqueness of mobility traces [9], which our analysis showed to be correlated with the success of MIA. For TFL, we group nearby stations – with the group size being a parameter which we configure in the set $\{5, 10, 20\}$ – and compute their combined aggregates. We find that, only when 20 stations are grouped together, there is a small increase in PG (0.30 on average), with few outliers reaching higher protection.

For SFC, we use grids of different spatial resolution to divide up the 30mi² area of downtown San Francisco, ranging from a baseline 10×10 grid resulting in ROIs of 0.3mi², to one single ROI of 30.3mi² (with the intermediate grid sizes being 5×5 and 2×2). Only when we consider a single ROI (1×1 grid) the PG increases slightly (0.25 on average), nonetheless, $PG \leq 0.23$ for 75% of the cabs. This means that the temporal dimension of the location contains enough information for the attack to succeed, when the adversary has the ‘Subset of Locations’ prior. In other words, such an attacker can perform MIA on the SFC dataset *even without any spatial information*.

Temporal Generalization (TG). We then vary the length of each timeslot from 1 hour (the baseline) to 1 week, keeping the original spatial resolution. For TFL, MIA’s performance only decreases significantly with 1-week granularity, increasing PG to 0.31 on average with few outliers. That is, *regular commuting patterns remain distinguishable in the aggregates even for relatively long periods of time*. In SFC, the attack’s performance starts degrading earlier (i.e., $PG=0.15$ for 1 day resolution), and while PG reaches 0.35 with a 1-week timeslot, it remains less than 0.27 for 25% of the cabs. This means that just 1 time point may be sufficient for the attack to succeed. Overall, even without the temporal dimension, the spatial domain still contains enough information to perform inference.

In theory, if one simultaneously generalized both time and space, MIA would be successfully mitigated; e.g., for 1×1 grid with 1-week temporal resolution, PG reaches 0.96 for SFC. However, in such a setting, the aggregates are not useful at all (see discussions in Section 5).

Data Generalization (DG). Finally, we experiment with releasing *ranges*: for instance, rather than reporting that 124 users were in a given ROI during a 1-hour timeslot, the range ‘120–130’ is published.

Data Generalization with Fixed Ranges (DGFR). We fix the interval size (denoted as x) w.r.t. the group size parameter m , i.e., we vary the interval based on the minimum and maximum possible values of the overall aggregates (as indicated by m). Then, we assign the location counts to the median of a range interval. For TFL, we range x in the set $\{2, 5, 10, 50, 150, 9,500\}$. We observe a significant gain for $x \in \{5, 10\}$, with 50% of the commuters obtaining gains $0.45 \leq PG \leq 0.6$ and $0.7 \leq PG \leq 0.8$, respectively. When $x=9,500$, i.e., the maximum possible count a location could have, there is no variance in the data and MIA becomes impossible, yielding $PG=1$. For SFC ($x \in \{2, 5, 10, 50, 100, 250\}$), DGFR requires larger intervals to have an effect on PG. For instance, when $x=50$ the PG highly varies ($0.35 \leq PG \leq 0.8$ for 50% of the cabs) and grows slowly and more consistently as x increases (mean PG 0.68 when $x=100$) until reaching $PG=1$ for all users when using the maximum possible interval ($x=250$).

Data Generalization with Adaptive ranges (DGAR). We also evaluate an adaptive approach to select the range interval for each location based on its minimum and maximum value over time. By tailoring the range to the locations, we expect to obtain better utility results (see Section 5). This approach is parameterized by $x' \in \{1, 2, 4, 8, 16\}$, which indicates the number of buckets released *per location* time-series. For TFL, publishing 1 or 2 buckets per location time-series results in a mean privacy gain of 0.91 and 0.71, respectively. When increasing x' , PG decreases: with $x'=4$ a few outliers are no longer protected from MIA. Similarly, for SFC, publishing 1 bucket per location yields a PG between 0.55 and 0.85 for 50% of the cabs, while with $x'=2$, the mean PG already drops to 0.25. This means that, as soon as information about the evolution of the location aggregates over time is revealed, cabs begin to be exposed to the attack.

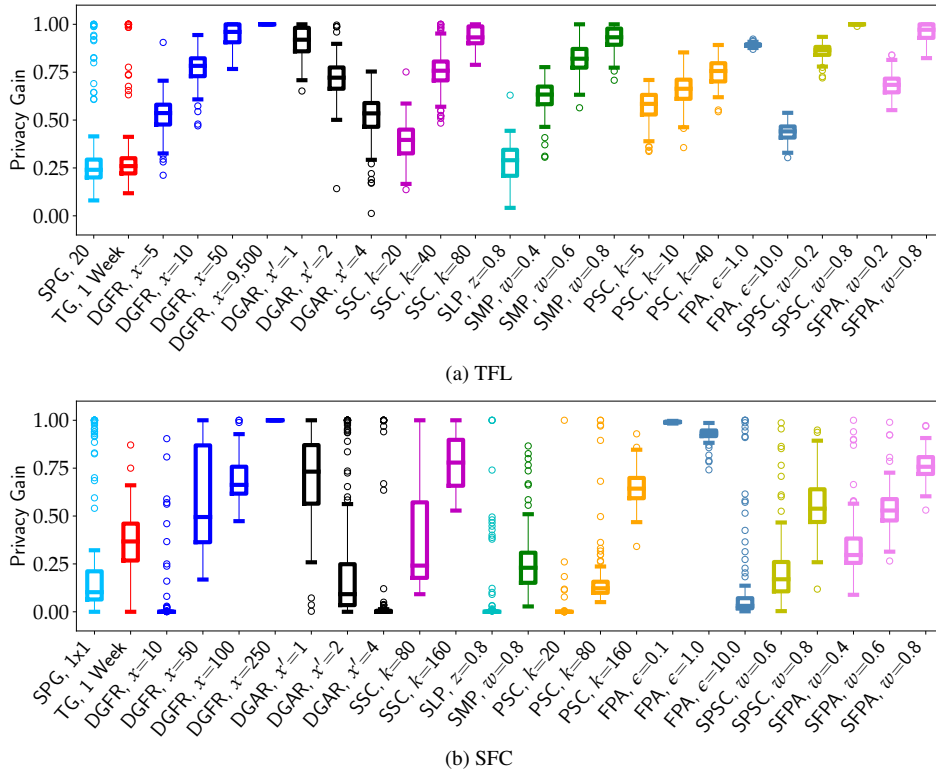


Figure 7: Privacy Gain for Various Defenses & Parameters.

4.2.2 Hiding

Another common approach used in location privacy literature is to hide (i.e., exclude) some spatio-temporal data points, by either suppressing or sampling them [19, 43]. Typically, *sensitive* points are removed and the released locations are not perturbed with any kind of noise.

Suppressing Small Counts (SSC). We first try suppressing points with small counts, i.e., replacing the points of the aggregate location time-series that do not exceed a certain threshold k with zeros. This approach satisfies the notion of $(k, 0)$ -crowd-blending privacy, introduced by Gehrke et al. in [11].² For TFL ($k \in \{2, 5, 10, 20, 40, 80\}$), suppressing counts with values smaller than 10 does not yield any privacy protection. As k increases, we do observe some gain in privacy; e.g., $PG=0.38$ for $k=20$, reaching 0.75 (resp., 0.93) when k is set to 40 (resp., 80). The SFC dataset is much denser, thus, it requires higher k to provide protection (we configure $k \in \{2, 5, 10, 20, 40, 80, 160\}$). Surprisingly, only when $k=80$ the PG increases to 0.4 on average, remaining smaller than 0.2 for 25% of the cabs. For $k=160$, mean PG increases to 0.78 while it is greater than 0.5 for most cabs.

Suppressing Less Popular Locations/Timeslots (SLP). Inspired by the result of the feature analysis in Section 3, which shows that some commuters/cabs are more “distinguishable” in the aggregates because they contribute events in less popular locations or times, we also experiment suppressing those

data points. We consider suppressing a percentage $z \in \{0.2, 0.4, 0.6, 0.8\}$ of the least popular locations and timeslots. However, despite the insight provided by our feature analysis, this technique does *not* actually provide significant gains. For instance, in TFL, suppressing 80% of the least popular locations/timeslots still yields a PG between 0.2 and 0.3 for 50% of the oysters. Similarly, in SFC, only some outliers are protected when we retain 20% of the most popular locations/timeslots (i.e., $z=0.8$). This fact reinforces the conclusion that the counts of the busiest locations/times contain information that help MIA.

Sampling (SMP). In Section 3, we also showed that a factor playing a part in the success of MIA is the amount of data users contribute to the aggregation. Therefore, we consider sampling as a means to reduce the amount of users’ data. We remove a percentage $w \in \{0.2, 0.4, 0.6, 0.8\}$ of users’ data points at random, and release the aggregate location time-series computed on the sampled trajectories. For TFL, this defense offers some privacy protection: the mean PG is 0.6 when $w=0.4$ (with only a few outliers not so well protected), and increases up to 0.9 when removing 80% of the users’ points. Thus, sampling might be a promising defense strategy against MIA on sparse datasets. On the contrary, this approach does not work nearly as well on the denser SFC dataset. Here, PG is negligible even when 60% of the events are randomly removed, and is between 0.2 and 0.3 for 50% of the cabs when 20% of their points are retained.

4.2.3 Perturbation

Next, we study the effect of perturbing the values of the aggregate location time-series, with carefully crafted *noise*. The

² k -crowd-blending sanitization ensures that the data of each individual u in a database *blends* with that of $k - 1$ other individuals, i.e., the output of a sanitization mechanism is *indistinguishable* if u ’s data is replaced by that of any of the other individuals.

state-of-the-art method for releasing aggregate statistics free from inferences is to satisfy differential privacy (DP) [10]. In this setting, Acs and Castelluccia [1] specify an algorithm tuned to the density of Paris for releasing aggregates statistics from a telecommunication service provider’s dataset, while Quercia et al. [38] use randomized response to let an untrusted aggregator privately learn the number of people in geographic locations. However, previous work [37, 36, 46] has shown that DP techniques ultimately yield poor utility on high-dimensional settings. To mitigate this problem, the noise addition can be configured to achieve weaker privacy guarantees, such as crowd-blending privacy [11], while retaining better utility levels. For instance, To et al. [46] apply this notion to release privacy-preserving location entropy statistics.

Perturbing Small Counts (PSC). We first add noise sampled from the Laplace distribution with scale $O(1/\epsilon')$ only to small counts, i.e., counts of the aggregate location time-series that are smaller than a threshold k . This achieves (k, ϵ') -crowd-blending privacy [11]. We range k as in Section 4.2.2 (SSC) and configure ϵ' to 1.0 for TFL and to 0.1 for the SFC dataset, since we expect that the denser SFC dataset requires larger scale noise addition to obtain some privacy protection. For TFL, this approach results in reasonable privacy gain. For instance, with $k=5$ the mean PG is 0.55 (with some outliers having less protection), while with $k=40$ the PG is higher than 0.6 for all commuters. On the contrary, for SFC, this mechanism does not offer much protection unless $k=160$, where $0.6 \leq \text{PG} \leq 0.7$ for 50% of the cabs.

Fourier Perturbation Algorithm (FPA). We then experiment with FPA [39], a differentially private mechanism tailored to time-series settings (see Appendix A for the algorithm’s description). We set ϵ in the range $\{0.01, 0.1, 1.0, 10.0\}$. As expected, PG is higher for smaller values of ϵ (i.e., stronger DP privacy guarantees). For TFL, with $\epsilon \leq 0.1$ PG reaches 1.0, while with $\epsilon=1.0$ it is above 0.85 for all the users. For larger values of ϵ , (i.e., 10.0), PG drops between 0.4 and 0.5 for 50% of the commuters. Similarly, for SFC, the mean PG is very high for ϵ values up to 1.0 (e.g., $\text{PG} \geq 0.75$ for all the cabs when $\epsilon=1.0$) but only a few outliers are well protected when $\epsilon=10.0$.

4.2.4 Combining Hiding and Perturbation

Finally, we investigate whether combining defense strategies can improve the privacy gain. In particular, we focus on the combination of sampling with perturbation which has been suggested in previous work [11, 26]. For instance, Gehrke et al. [11] show that introducing a random sampling step before the application of a crowd-blending privacy mechanism (e.g., PSC) achieves a stronger privacy notion, namely, zero-knowledge privacy [12].³ Similarly, Li et al. [26] suggest that a random sampling step can amplify the privacy offered by a differentially private mechanism, thus, we also combine sampling with FPA.

Sampling & Perturbing Small Counts (SPSC). For TFL, we

³A zero-knowledge private mechanism applied on a database does not release any additional information beyond some *aggregate information* that is acceptable to publish.

set k to 5 and ϵ' to 1.0, while for SFC, we set k to 20 and ϵ' to 0.1. For both datasets, we range the sampling parameter w in $\{0.2, 0.4, 0.6, 0.8\}$. We find that the introduction of a random sampling step boosts the PG of the perturbation mechanism. For TFL, when we retain 80% of the data (i.e., $w=0.2$), the PG is higher than 0.68 for all the users and 0.85 on average. This is a $4\times$ and $2\times$ increase compared to SMP or PSC alone. Furthermore, with $w=0.6$ or 0.8, PG almost reaches 1. On the SFC dataset, we observe once again that more data needs to be removed to obtain some PG for the cabs. In particular, sampling boosts the mean privacy gain to 0.21 when $w=0.6$, a $4\times$ or $21\times$ increase compared to SMP and PSC alone. When we set w to 0.8, PG is between 0.45 and 0.6 for 50% of the cabs.

Sampling & Fourier Perturbation Algorithm (SFPA). For both datasets, we configure FPA’s privacy budget ϵ to the least conservative setting, i.e., $\epsilon=10.0$, while varying w , to observe its amplifying effect on PG. For TFL, when we retain 80% of the data (i.e., $w=0.2$) the mean PG is 0.68, which is approx. 2.5 times or 1.5 times higher than SMP or FPA, respectively, alone. As we increase w , the PG is increasing further, e.g., with $w=0.8$ $\text{PG} \geq 0.8$ for all commuters. For SFC, higher sampling rates are required to obtain similar privacy levels. When $w=0.4$, a few outliers are not protected from MIA while when $w=0.8$, $0.7 \leq \text{PG} \leq 0.8$ for 50% of the cabs.

4.3 Unsuitable Defenses

In theory, one could attempt to add *dummy* locations to obfuscate users’ trajectories [30]. However, it is well-known that generating plausible dummy locations is extremely hard, as those can be easily filtered by the adversary by exploiting statistical correlations with real locations, and thus ultimately provide no protection [8].

Another possible approach would be to generate and use *synthetic traces* [3, 28, 17, 15, 31], and compute the statistics on them, rather than on the actual locations of the users. However, when attempting to implement and evaluate these methods, we found that the synthetic trajectories generated using techniques presented in [17, 15] do not preserve the time dimension, while those proposed in [28, 31] only work for one specific analytic task—namely, computing origin-destination commute distances.

Bindschaedler and Shokri [3] support *plausible deniability* with respect to whether a real trace (a “seed”) was part of the training set used by a privacy-preserving generative model to produce synthetic traces. Given a set of synthetic traces, an adversary cannot learn which locations the seed contributors have visited or whether a user with certain semantic habits is in the seed dataset. This is a different goal than the one we consider, i.e., given aggregate location statistics, preventing an adversary from inferring whether a user contributed to them. Moreover, when the goal is to release traces [3], one can afford to aggressively sample points from the trajectories in order to make the system scale. Whereas, we cannot do so since, in the use cases considered in our paper, we need fine-grained statistics. Not using aggressive sampling remarkably increases the computational cost of the generation process and ultimately

makes it impossible to properly evaluate [3]’s approach in our setting.

4.4 Take Aways

Overall, our experiments show that, *spatio-temporal generalization*, a technique commonly used to protect privacy for mobility trajectories [25, 14, 9], does not yield meaningful protection against MIA on aggregate location time-series, since both dimensions contain information that is useful for the attack. On the contrary, *data generalization* approaches like discretizing the counts of the time-series can actually provide acceptable privacy levels. However, the protection obtained for a discretization level is data-dependent, thus, it is not possible to have a universal mechanism to configure the mechanism other than doing an ad-hoc privacy analysis.

We also find that *hiding* techniques (e.g., suppression or sampling) yield higher privacy levels when the input signal is sparse (as for TFL), but do not work as well on dense datasets (SFC). Regardless, suppressing locations/timeslots based on popularity does not improve privacy, indicating that busy ROIs/times contribute significantly to the attack.

Finally, *perturbation* techniques configured to guarantee differential privacy achieve, as expected, very high gains in privacy. However, similar levels of protection can be reached with less noise using techniques like crowd-blending sanitization. Also, combining both sampling and perturbation can significantly amplify the defenses’ privacy gain.

5 Privacy–Utility Trade-off

We now study the impact of the defense strategies on *utility*, for different levels of privacy protection. Privacy is again quantified via the ability of mitigating MIA (i.e., the Privacy Gain), while we measure utility vis-à-vis analytics tasks that may rely on aggregate location time-series: (1) forecasting traffic volumes in Regions of Interest [21, 18], (2) mining interesting locations or discovering hotspots [55, 23], (3) map inference [27], and (4) detecting mobility anomalies [35]. To represent each analytics setting, we consider utility metrics that capture the key characteristics of the aggregate data enabling that application. In Figures 8–11, we plot the privacy gain vs. the utility loss for each task (i.e., the decrease in utility compared to performing the same task on raw aggregate location time-series).⁴ Ideally, we would like to obtain data points on the upper left corner of the plots, i.e., where the privacy gain is high and the utility loss is low.

5.1 Forecasting Traffic: Aggregates Error

Aggregate location time-series are often used for forecasting traffic in ROIs [21, 18]. We measure the utility loss by quantifying the effect of a defense on the *precision* of the data release, i.e., the error the defense introduces, as that would inevitably effect the forecast as well. We use the Mean Relative Error (MRE) over the whole time-series or a percentage thereof (e.g., the MRE over the 10% busiest ROIs). Given two

time-series Y and Y' , of length $|\mathcal{T}|$, denoting the aggregates before and after a defense has been applied, we calculate:

$$\text{MRE}(Y, Y') = \frac{1}{|\mathcal{T}|} \sum_{t \in \mathcal{T}} \frac{|Y'_t - Y_t|}{\max(\gamma, Y_t)} \quad (2)$$

(γ is a sanity bound mitigating the effect of very small counts).

Figure 8 plots the results for this task. For TFL, defenses like data generalization with adaptive ranges (DGAR), sampling alone (SMP) or combined with FPA perturbation (SFPA), and small count suppression (SSC), yield reasonable privacy–utility trade-offs (Figure 8a). If one is interested in performing predictive analytics only on the busiest stations (e.g., MRE 10% – Figure 8b), defenses such as perturbing small counts (PSC) or data generalization with fixed ranges (DGFR) yield better trade-offs, with the former performing better than the latter in terms of utility (but worse for privacy). In this setting, if slightly higher utility loss can be tolerated, sampling and perturbation of small counts (SPSC) as well as FPA can provide better privacy (i.e., PG between 0.8 and 1.0).

For SFC, DGAR or SSC yield small MRE overall (Figure 8c) and could be used well for predictive analytics. Nonetheless, to forecast traffic in the top 10% of SFC regions (Figure 8d), FPA or PSC yield an efficient privacy–utility trade-off balance (0.9 PG and 10^{-2} utility loss for the former and 0.64 PG and $9 \cdot 10^{-3}$ utility loss for the latter).

5.2 Hotspot Discovery: Prediction Accuracy & Rank Correlation

Analysts are often interested in predicting *location hotspots* over time [55]; this is particularly useful for journey planning and/or resource allocation. For instance, authorities need to learn which stations are the busiest in certain hours of a day to allocate staff accordingly, or to suggest alternative routes to commuters. Hotspot discovery is also crucial to identify the optimal location and time to place advertisements, open new shops, etc. [45, 23]. For this task, we measure utility as follows: we use the aggregates after applying a defense to predict the busiest 10% ROIs at each timeslot of the inference week, and calculate the F1 score of the predictions:

$$\text{F1} = 2 \cdot \frac{\text{PPV} \cdot \text{TPR}}{\text{PPV} + \text{TPR}} \quad (3)$$

where $\text{PPV} = \frac{\text{TP}}{\text{TP} + \text{FP}}$ is the precision and $\text{TPR} = \frac{\text{TP}}{\text{TP} + \text{FN}}$ is the recall of the predictions, with TP, FP and FN indicating the true/false positives and false negatives, respectively.

Note that the F1 score quantifies how successful hotspot prediction is in each timeslot, but does not capture if the ordering of the hotspots is preserved. This might be important for resource planning, e.g., a taxi company assigning vehicles to locations sorted by client demand. Thus, we also calculate the Kendall rank correlation coefficient, a measure of correspondence between two rankings, whereby values closer to 1 indicate strong agreement and those closer to -1 strong disagreement. More precisely, given two rankings, X and X' , the Kendall rank correlation $\tau(X, X')$ is computed as:

$$\tau(X, X') = \frac{P - Q}{\sqrt{(P + Q + T) \cdot (P + Q + U)}} \quad (4)$$

⁴In Appendix B, we report several tables indicating how the configuration of each defense affects the utility metrics under consideration.

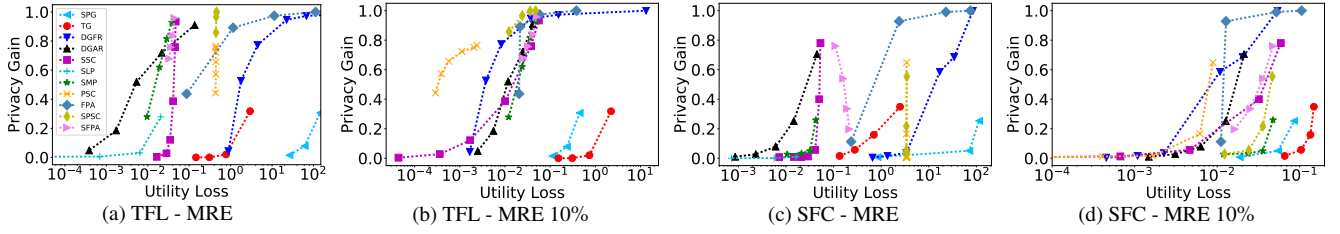


Figure 8: Privacy–Utility Trade-off: Forecasting Traffic (Aggregates Error).

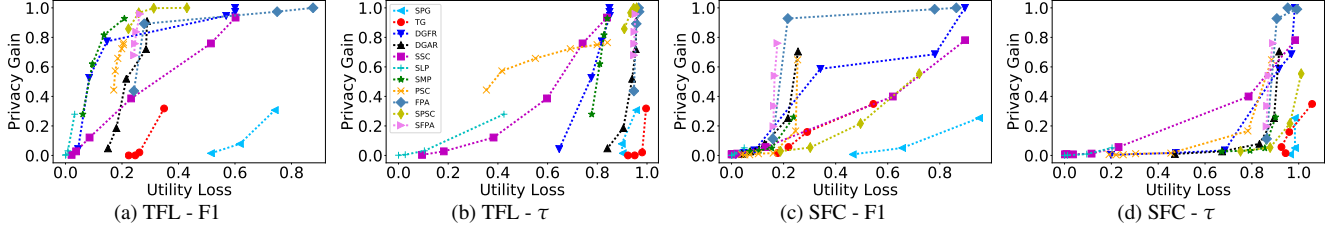


Figure 9: Privacy–Utility Trade-off: Hotspot Discovery (Prediction Accuracy & Rank Correlation).

where P is the number of concordant pairs, Q that of discordant pairs, T the number of ties only in X , and U the number of ties only in X' . If a tie occurs for the same pair in both X and X' , it is not added to either T or U [24].

In the case of TFL, Figure 9a shows that DGFR and SMP have small utility loss (0.1–0.15) and relatively high privacy gain (0.5–0.8), indicating that they are indeed suitable for hotspot discovery tasks. However, if the ranking of the top stations is crucial, then, defense strategies such as SSC or PSC outperform the others (Figure 9b). In SFC, for hotspot prediction, FPA and SFFPA perform best as they yield higher PG for similar levels of utility. The same observation holds for ranking the top locations (Figure 9d), even though SSC could be used if one is willing to sacrifice some privacy for slightly better utility (0.4 PG and 0.75 utility loss).

5.3 Map Inference: Distribution Similarity

Tasks like map inference – i.e., inferring road maps from GPS traces [27] or labeling locations [53] – rely on the fact that certain locations are more frequently visited than others [3]. Thus, to evaluate utility in this setting, we use the Jensen-Shannon (JS) divergence, which estimates the similarity between two probability distributions. This captures whether the distribution of location visits is preserved (for each timeslot) after applying a defense. JS is a smoothed version of the Kullback-Leibler (KL) that is symmetric and always defined. Given two probability distributions, V and W , the JS-divergence is calculated as:

$$JS(V||W) = \frac{1}{2} \cdot KL(V||Z) + \frac{1}{2} \cdot KL(W||Z) \quad (5)$$

where $Z = \frac{1}{2} \cdot (V + W)$. JS is a value between 0 and 1 with larger values indicating bigger distance between the distributions (i.e., worse utility for map inference).

Figure 10 visualizes the privacy–utility trade-off of the various defenses for map inference tasks, for both datasets. For TFL, Figure 10a shows that a few defenses, including sampling without or with FPA (SMP or SFFPA), DGAR, PSC, and SPSC do achieve good trade-offs. For instance, sampling yields a

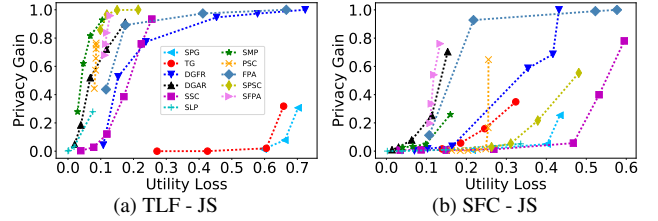


Figure 10: Privacy–Utility Trade-off: Map Inference (Distribution Similarity).

0.06 utility loss for a mean privacy gain of 0.8, while, when combined with small count perturbation, PG reaches 0.96 for a utility loss of 0.11. For SFC, DGAR as well as SFFPA yield privacy gains between 0.25 and 0.75 with approx. 0.1 utility loss (Figure 10b). Higher privacy levels achieved by FPA or DGFR only come with increase in utility loss, while other defenses such as sampling with small count perturbation or small count suppression (SPSC or SSC) yield worse utility without actually improving privacy.

5.4 Anomaly Detection: Correlation

Finally, analytics aiming to detect mobility anomalies [33] and/or improve traffic forecasting in the presence of an anomaly, require that a linear relationship between two time-series—before and after applying a defense—is preserved [35]. Thus, here we calculate the Pearson correlation coefficient between the perturbed and raw aggregate time-series to measure utility. The Pearson correlation varies between -1 and $+1$, with values closer to 1 indicating positive linear correlation, and to -1 total negative correlation (values close to 0 imply no linear correlation). Given two signals Y and Y' , the Pearson correlation is computed as:

$$r(Y, Y') = \frac{\sum(Y - \mu_Y) \cdot (Y' - \mu_{Y'})}{\sqrt{(\sum(Y - \mu_Y)^2) \cdot (\sum(Y' - \mu_{Y'})^2)}} \quad (6)$$

where μ_X is the mean of a signal X .

In the TFL setting, data generalization with adaptive ranges (DGAR) and sampling (SMP) offer a reasonable balance in the trade-off (Figure 11a), while other defenses, such as FPA,

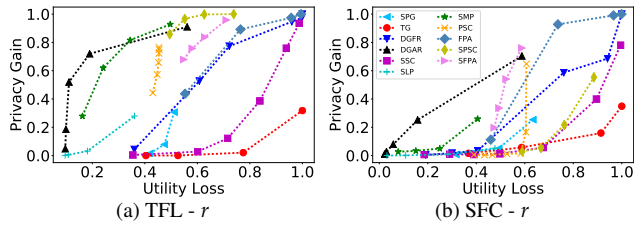


Figure 11: Privacy-Utility Trade-off: Anomaly Detection (Correlation).

data generalization with fixed ranges (DGFR), and small count suppression (SSC), increase privacy only if breaking the correlations. For SFC (Figure 11b), FPA with or without sampling yields, resp., 0.75 PG with 0.6 utility loss and 0.92 PG with 0.7 utility loss. In this case, DGAR achieves smaller utility loss (0.18) with some decrease in privacy gain (0.25).

5.5 Take Aways

The analysis presented in this section shows that defenses yield variable trade-offs for different analytics. There are defenses, such as spatio-temporal generalization, that not only yield poor utility, but also do not protect privacy. Other defenses, e.g., suppressing locations/timeslots based on their popularity, generally yield good utility for the analytics under consideration, but they provide poor levels of privacy. Defenses like data generalization, small count suppression, sampling, perturbation, or combinations of the last two, can be configured to obtain reasonable privacy levels while still providing utility for certain applications. In particular, data generalization techniques enable analysts to perform forecasting traffic tasks, hotspot discovery, and map inference, while small count suppression can be useful towards ranking hotspots. Sampling can retain utility for tasks such as location labeling and anomaly detection, but, from a privacy perspective, they work better when the dataset is sparse.

Perturbation techniques configured to guarantee strong DP achieve reasonable accuracy for applications such as discovering hotspots and forecasting their traffic, while additional tasks, e.g., forecasting the traffic of less busy ROIs or detecting anomalies, are more efficient when the injected noise is tailored to achieve weaker privacy notions (e.g., crowd-blending privacy). Interestingly, our results show that combining defenses, e.g., sampling and perturbation, not only helps privacy, but also retains utility for tasks such as ranking hotspots, map inference, and anomaly detection.

In conclusion, our evaluation highlights that there is no silver bullet against MIAs on aggregate location time-series and the design of a generalizable and robust defense is very challenging. However, for specific tasks and datasets, it is possible to select and configure defenses that provide acceptable utility to analysts without being detrimental to privacy—our extensive evaluations show why and how.

6 Related Work

Location Privacy. Golle and Partridge [13] demonstrate the feasibility of re-identifying users by leveraging the uniqueness of their home/work places. Shokri et al. [44] show that

k-anonymity in the context of location traces is mostly ineffective, while Zang and Bolot [54] that anonymization of location data is, in general, extremely difficult. De Montjoye et al. [9] measure the uniqueness of human mobility in a Call Detail Records (CDR) dataset, finding that four spatio-temporal points are enough to uniquely identify 95% of the individuals. They also show that coarsening the data, both spatially and temporally, does not add significant anonymity.

We have also discussed and experimented with defense techniques based on generalization [14, 6, 49] and hiding [19, 43]; although some of these efforts also focus on understanding which characteristics of location data threaten user privacy, they do so for *single users'* location traces—a different setting than aggregate location time-series.

Aggregate location privacy. Aggregation is often not an effective way to preserve the privacy of location data, as aggregates leak information about individual users. Xu et al. [52] reconstruct victims' location trajectories from aggregate mobility data, without any prior knowledge, while [36] shows that aggregate location time-series can be used by an adversary to build accurate profiles of users' movements. Finally, Boukoros et al. [4] study the effect of defenses on finding points of interest while computing aggregated statistics of geo-located measurements; in this work, we focus on a different privacy violation, i.e., membership inference.

Membership inference on aggregate locations. As discussed in Section 2.2, Pyrgelis et al. [37] model MIAs against aggregate locations using a distinguishability game, and train a classifier to differentiate aggregates including the data of a target from those that do not. While our analysis is based on their attacks, our research objective is substantially different. Pyrgelis et al.'s main goal is to investigate the feasibility of inference attacks; whereas, we aim to gain a deeper understanding about the reasons behind the attacks' success, providing insights about locations and times that ease inference and the characteristics of the users that are affected more than others. Moreover, [37] only studies the utility-privacy trade-off provided by differential privacy [39, 10], while we use the insights obtained in our analysis to select potential mitigation approaches, which we evaluate, both in terms of privacy and utility, in the context of various spatio-temporal analytics tasks.

MIAs in other settings. In [20], Homer et al. show that aggregate genomic statistics leak information about the inclusion of a target's genome in the dataset. Then, Wang et al. [50] improve on the attack by taking into account correlations within the human genome, while Backes et al. [2] generalize the attack to other types of data like microRNA expression datasets. The data targeted by these studies does not have spatio-temporal dimensions, and thus they are orthogonal to our work. Buscher et al. [5] study MIAs in the context of smart-metering, showing how aggregating a small number of household readings does not protect the privacy of individual (house) profiles. While smart metering data is also a time-series, it does not have spatial components, and the correlations are different. Finally, previous work studies membership inference on machine learning models, i.e., learning whether a data point was used to train a model, using the intuition that

the model ends up overfitting on data used for training [41]. The attack is also effective under less restrictive adversarial assumptions [40] and feasible in broader scenarios. Hayes et al. [16] show that MIAs are also possible against generative models, while Melis et al. [29] do so for collaborative and federated learning. Protection mechanisms against MIA on machine learning, such as dropout or model stacking [40], or adversarial training [32], cannot be applied in our scenario since the aggregate publication does not involve learning. Thus, studies that aim at understanding why membership on machine learning works [47] cannot inform defenses for aggregate location time-series.

7 Conclusion

In this paper, we conducted the first in-depth study of why and how membership inference attacks on location aggregates are successful, aiming to inform the design of defenses that maintain the utility of the statistics. We found that both regular and uncommon mobility patterns are the easiest to recognize. Also, size matters: users contributing a lot of data to the aggregates are easier to attack. However, there is no characteristic that can be singled out and eliminated to thwart the attack. Thus, it is unlikely that a unique generic defense can preserve the utility of the analytics for arbitrary applications. Nonetheless, our evaluation of defenses for a range of applications and mobility profiles shows that it is possible to design ad-hoc effective defenses that provide reasonable utility. For instance, data generalization techniques can be used for traffic forecasting and anomaly detection tasks, while hotspot discovery and map inference can be supported via sampling or perturbation on sparse and dense datasets, respectively.

Our study of defenses, while comprehensive, is inevitably limited to adapting existing location privacy defenses, and to a subset of parameters. Thus, it remains an open question whether new ad-hoc strategies tailored to counter MIA could provide a better privacy-utility trade-off for one application, or even a wider range of mobility analytics. A promising option is the use of differentially private noise highly tuned for a specific task. Another avenue to explore is the generation of synthetic data tailored to mobility analytics that rely on aggregates instead of trajectories, i.e., schemes that preserve space and time and granularity while still providing privacy. As a starting point for this line of research, we make the source code of all our experiments and implementations available upon request, hoping that they will serve as a building block for tools helping analysts and data providers to select the right defense mechanism. In future work, we also plan to release APIs providing easy access to various defense strategies and to investigate the effectiveness of defenses against privacy violations other than membership inference.

References

[1] G. Acs and C. Castelluccia. A case study: Privacy-preserving release of spatio-temporal density in Paris. In *KDD*, 2014.
 [2] M. Backes, P. Berrang, M. Humbert, and P. Manoharan. Membership privacy in MicroRNA-based studies. In *CCS*, 2016.

[3] V. Bindschaedler and R. Shokri. Synthesizing plausible privacy-preserving location traces. In *S&P*, 2016.
 [4] S. Boukoros, M. Humbert, S. Katzenbeisser, and C. Troncoso. Why Johnny Can't Develop Mobile Crowdsourcing Applications with Location Privacy. *arXiv:1901.04923*, 2019.
 [5] N. Buscher, S. Boukoros, S. Bauregger, and S. Katzenbeisser. Two Is Not Enough: Privacy Assessment of Aggregation Schemes in Smart Metering. In *PoPETS*, 2017.
 [6] X. Cai, R. Nithyanand, T. Wang, R. Johnson, and I. Goldberg. A systematic approach to developing and evaluating website fingerprinting defenses. In *CCS*, 2014.
 [7] L. Canzian and M. Musolesi. Trajectories of depression: unobtrusive monitoring of depressive states by means of smartphone mobility traces analysis. In *Ubicomp*, 2015.
 [8] R. Chow and P. Golle. Faking contextual data for fun, profit, and privacy. In *WPES*, 2009.
 [9] Y.-A. de Montjoye, C. A. Hidalgo, M. Verleysen, and V. D. Blondel. Unique in the Crowd: The privacy bounds of human mobility. *SREP*, 2013.
 [10] C. Dwork. Differential privacy: A survey of results. In *TAMC*, 2008.
 [11] J. Gehrke, M. Hay, E. Lui, and R. Pass. Crowd-blending privacy. In *CRYPTO*, 2012.
 [12] J. Gehrke, E. Lui, and R. Pass. Towards privacy for social networks: A zero-knowledge based definition of privacy. In *TCC*, 2011.
 [13] P. Golle and K. Partridge. On the Anonymity of Home/Work Location Pairs. In *Pervasive Computing*, 2009.
 [14] M. Gruteser and D. Grunwald. Anonymous Usage of Location-Based Services Through Spatial and Temporal Cloaking. In *MobiSys*, 2003.
 [15] M. E. Gursoy, L. Liu, S. Truex, L. Yu, and W. Wei. Utility-aware synthesis of differentially private and attack-resilient location traces. In *CCS*, 2018.
 [16] J. Hayes, L. Melis, G. Danezis, and E. De Cristofaro. LOGAN: Evaluating Privacy Leakage of Generative Models Using Generative Adversarial Networks. *arXiv 1705.07663*, 2017.
 [17] X. He, G. Cormode, A. Machanavajjhala, C. M. Procopiuc, and D. Srivastava. Dpt: differentially private trajectory synthesis using hierarchical reference systems. *VLDB*, 2015.
 [18] M. X. Hoang, Y. Zheng, and A. K. Singh. Forecasting Citywide Crowd Flows based on Big Data. In *SIGSPATIAL*, 2016.
 [19] B. Hoh, M. Gruteser, H. Xiong, and A. Alrabady. Preserving privacy in GPS traces via uncertainty-aware path cloaking. In *CCS*, 2007.
 [20] N. Homer, S. Szlinger, M. Redman, D. Duggan, W. Tembe, J. Muehling, J. V. Pearson, D. A. Stephan, S. F. Nelson, and D. W. Craig. Resolving individuals contributing trace amounts of DNA to highly complex mixtures using high-density SNP genotyping microarrays. *PLoS Genetics*, 2008.
 [21] R. Jiang, X. Song, Z. Fan, T. Xia, Q. Chen, Q. Chen, and R. Shibasaki. Deep ROI-Based Modeling for Urban Human Mobility Prediction. *IMWUT*, 2018.
 [22] I. Jolliffe. *Principal Component Analysis*. Wiley & Sons, 2002.
 [23] D. Karamshuk, A. Noulas, S. Scellato, V. Nicosia, and C. Mascolo. Geo-spotting: mining online location-based services for optimal retail store placement. In *KDD*, 2013.
 [24] M. G. Kendall. The treatment of ties in ranking problems. *Biometrika*, 1945.
 [25] J. Krumm. Inference attacks on location tracks. In *PerCom*. Springer, 2007.
 [26] N. Li, W. Qardaji, and D. Su. On sampling, anonymization, and differential privacy or, k-anonymization meets differential

- privacy. In *ASIACCS*, 2012.
- [27] X. Liu, J. Biagioni, J. Eriksson, Y. Wang, G. Forman, and Y. Zhu. Mining large-scale, sparse gps traces for map inference: comparison of approaches. In *KDD*, 2012.
- [28] A. Machanavajjhala, D. Kifer, J. Abowd, J. Gehrke, and L. Vihuber. Privacy: Theory meets practice on the map. In *ICDE*, 2008.
- [29] L. Melis, C. Song, E. De Cristofaro, and V. Shmatikov. Inference attacks against collaborative learning. *arXiv 1805.04049*, 2018.
- [30] J. Meyerowitz and R. R. Choudhury. Hiding Stars with Fireworks: Location Privacy Through Camouflage. In *MobiCom*, 2009.
- [31] D. J. Mir, S. Isaacman, R. Cáceres, M. Martonosi, and R. N. Wright. Dp-where: Differentially private modeling of human mobility. In *BigData*, 2013.
- [32] M. Nasr, R. Shokri, and A. Houmansadr. Machine learning with membership privacy using adversarial regularization. *arXiv 1807.05852*, 2018.
- [33] B. Pan, Y. Zheng, D. Wilkie, and C. Shahabi. Crowd sensing of traffic anomalies based on human mobility and social media. In *SIGSPATIAL*, 2013.
- [34] M. Piorkowski, N. Sarafijanovic-Djukic, and M. Grossglauser. CRAWDAD EPFL/Mobility Dataset. <http://crawdad.org/epfl/mobility/20090224>, 2009.
- [35] A. Pyrgelis, E. De Cristofaro, and G. J. Ross. Privacy-friendly mobility analytics using aggregate location data. In *SIGSPATIAL*, 2016.
- [36] A. Pyrgelis, C. Troncoso, and E. De Cristofaro. What Does The Crowd Say About You? Evaluating Aggregation-based Location Privacy. In *PoPETS*, 2017.
- [37] A. Pyrgelis, C. Troncoso, and E. De Cristofaro. Knock Knock, Who’s There? Membership Inference on Aggregate Location Data. In *NDSS*, 2018.
- [38] D. Quercia, I. Leontiadis, L. McNamara, C. Mascolo, and J. Crowcroft. SpotMe if you can: Randomized responses for location obfuscation on mobile phones. In *ICDCS*, 2011.
- [39] V. Rastogi and S. Nath. Differentially private aggregation of distributed time-series with transformation and encryption. In *SIGMOD*, 2010.
- [40] A. Salem, Y. Zhang, M. Humbert, M. Fritz, and M. Backes. ML-Leaks: Model and Data Independent Membership Inference Attacks and Defenses on Machine Learning Models. *arXiv 1806.01246*, 2018.
- [41] R. Shokri, M. Stronati, C. Song, and V. Shmatikov. Membership inference attacks against machine learning models. In *S&P*, 2017.
- [42] R. Shokri, G. Theodorakopoulos, G. Danezis, J.-P. Hubaux, and J.-Y. Le Boudec. Quantifying Location Privacy: The Case of Sporadic Location Exposure. In *PoPETS*, 2011.
- [43] R. Shokri, G. Theodorakopoulos, J.-Y. Le Boudec, and J.-P. Hubaux. Quantifying location privacy. In *S&P*, 2011.
- [44] R. Shokri, C. Troncoso, C. Diaz, J. Freudiger, and J.-P. Hubaux. Unraveling an old cloak: k-anonymity for location privacy. In *WPES*, 2010.
- [45] Telefonica Smart Steps. <https://www.business-solutions.telefonica.com/en/enterprise/solutions/smarter-selling/big-data-insights/>, 2019.
- [46] H. To, K. Nguyen, and C. Shahabi. Differentially private publication of location entropy. In *SIGSPATIAL*, 2016.
- [47] S. Truex, L. Liu, M. E. Gursoy, L. Yu, and W. Wei. Towards Demystifying Membership Inference Attacks. *arXiv 1807.09173*, 2018.
- [48] Uber Movement. <https://movement.uber.com/>, 2019.
- [49] G. Venkatadri, A. Andreou, Y. Liu, A. Mislove, K. P. Gummadi, P. Loiseau, and O. Goga. Privacy Risks with Facebook’s PII-based Targeting: Auditing a Data Brokers Advertising Interface. In *S&P*, 2018.
- [50] R. Wang, Y. F. Li, X. Wang, H. Tang, and X. Zhou. Learning your identity and disease from research papers: information leaks in genome wide association study. In *CCS*, 2009.
- [51] Waze. <https://www.waze.com>, 2019.
- [52] F. Xu, Z. Tu, Y. Li, P. Zhang, X. Fu, and D. Jin. Trajectory Recovery From Ash: User Privacy Is NOT Preserved in Aggregated Mobility Data. In *WWW*, 2017.
- [53] M. Ye, D. Shou, W.-C. Lee, P. Yin, and K. Janowicz. On the semantic annotation of places in location-based social networks. In *KDD*, 2011.
- [54] H. Zang and J. Bolot. Anonymization of location data does not work: A large-scale measurement study. In *MobiCom*, 2011.
- [55] Y. Zheng, L. Zhang, X. Xie, and W.-Y. Ma. Mining interesting locations and travel sequences from gps trajectories. In *WWW*, 2009.

A Fourier Perturbation Algorithm

The Fourier Perturbation Algorithm (FPA) [39] operates as follows: a time-series is first transformed to the frequency domain using the Discrete Fourier Transform (DFT), and l Fourier coefficients F_l are retained (l is an algorithm parameter). Then, F_l is perturbed with noise sampled from the Laplace distribution, with scale $O(\sqrt{l} \cdot \Delta f_2 / \epsilon)$ and padded with zeros to the size of the original time-series (note that Δf_2 depicts the ℓ_2 norm of the users’ sensitivity). Finally, the inverse DFT is performed on F_l to obtain the perturbed time-series. As discussed in [39], FPA provides ϵ -DP guarantees.

B Utility Metrics for Defenses

We report tables that demonstrate how each defense affects the various utility metrics that we consider. For ease of comparisons, Table 4 shows, for each of the considered metrics, the utility corresponding to a random guess.

Dataset	MRE	MRE 10%	F1	τ	JS	r
TFL	4285.809	13.267	0.099	0.002	0.733	-0.002
SFC	85.122	0.08	0.094	-0.001	0.472	0.001

Table 4: Utility metrics corresponding to a random guess.

Group Size	MRE	MRE 10%	F1	τ	JS	r
5	26.326	0.113	0.485	0.098	0.596	0.581
10	61.457	0.234	0.383	0.102	0.662	0.525
20	145.056	0.449	0.259	0.043	0.702	0.489

Table 5: TFL, Utility for Spatial Generalization (SPG).

Grid Size	MRE	MRE 10%	F1	τ	JS	r
5x5	0.840	0.019	0.534	0.036	0.215	0.684
2x2	71.270	0.055	0.344	0.016	0.402	0.507
1x1	114.199	0.086	0.049	0.017	0.434	0.367

Table 6: SFC, Utility for Spatial Generalization (SPG).

Timeslot	MRE	MRE 10%	F1	τ	JS	r
4 Hours	0.146	0.152	0.776	0.076	0.272	0.596
8 Hours	0.308	0.308	0.753	0.049	0.426	0.474
1 Day	0.777	0.741	0.738	0.020	0.605	0.225
1 Week	2.945	2.221	0.651	0.003	0.658	0.000

Table 7: TFL, Utility for Temporal Generalization (TG).

Timeslot	MRE	MRE 10%	F1	τ	JS	r
4 Hours	0.134	0.066	0.823	0.056	0.139	0.632
8 Hours	0.280	0.104	0.781	0.074	0.186	0.413
1 Day	0.703	0.135	0.709	0.040	0.246	0.086
1 Week	2.493	0.149	0.455	-0.057	0.324	0.000

Table 8: SFC, Utility for Temporal Generalization (TG).

x	MRE	MRE 10%	F1	τ	JS	r
2	0.884	0.002	0.955	0.353	0.108	0.640
5	1.779	0.004	0.916	0.224	0.153	0.393
10	4.472	0.008	0.853	0.182	0.238	0.278
50	22.516	0.037	0.431	0.150	0.453	0.040
150	67.673	0.153	0.399	0.151	0.578	0.003
9500	4281.495	13.261	0.400	0.151	0.724	0.000

Table 9: TFL, Utility for Data Generalization with fixed ranges of size x (DGFR).

x	MRE	MRE 10%	F1	τ	JS	r
2	0.659	0.000	0.983	0.802	0.070	0.809
5	1.358	0.001	0.953	0.525	0.103	0.700
10	3.385	0.002	0.911	0.316	0.164	0.594
50	17.012	0.011	0.658	0.084	0.354	0.239
100	34.214	0.020	0.218	0.031	0.416	0.059
250	84.667	0.054	0.103	0.017	0.432	0.000

Table 10: SFC, Utility for Data Generalization with fixed ranges of size x (DGFR).

x'	MRE	MRE 10%	F1	τ	JS	r
1	0.136	0.041	0.711	0.043	0.175	0.439
2	0.022	0.025	0.715	0.045	0.117	0.810
4	0.005	0.012	0.785	0.060	0.068	0.889
8	0.002	0.006	0.820	0.095	0.039	0.901
16	0.000	0.002	0.850	0.159	0.020	0.903

Table 11: TFL, Utility for Data Generalization with adaptive ranges and x' buckets (DGAR).

x'	MRE	MRE 10%	F1	τ	JS	r
1	0.045	0.021	0.745	0.083	0.153	0.412
2	0.015	0.013	0.783	0.106	0.113	0.842
4	0.006	0.006	0.873	0.167	0.063	0.943
8	0.002	0.003	0.928	0.327	0.030	0.971
16	0.001	0.001	0.961	0.529	0.014	0.978

Table 12: SFC, Utility for Data Generalization with adaptive ranges and x' buckets (DGAR).

k	MRE	MRE 10%	F1	τ	JS	r
2	0.016	0.000	0.978	0.905	0.039	0.646
5	0.028	0.000	0.962	0.818	0.078	0.399
10	0.035	0.002	0.915	0.618	0.119	0.285
20	0.041	0.010	0.767	0.402	0.171	0.162
40	0.045	0.038	0.485	0.259	0.224	0.061
80	0.047	0.056	0.398	0.161	0.256	0.012

Table 13: TFL, Utility for Suppressing Small Counts (SSC).

k	MRE	MRE 10%	F1	τ	JS	r
2	0.007	0.000	1.000	0.998	0.034	0.815
5	0.015	0.000	0.999	0.992	0.087	0.710
10	0.021	0.000	0.995	0.964	0.150	0.610
20	0.029	0.001	0.978	0.885	0.269	0.503
40	0.041	0.005	0.869	0.769	0.468	0.324
80	0.050	0.032	0.381	0.214	0.532	0.104
160	0.053	0.059	0.103	0.015	0.595	0.005

Table 14: SFC, Utility for Suppressing Small Counts (SSC).

z	MRE	MRE 10%	F1	τ	JS	r
0.2	0.000	0.0	1.000	1.000	0.000	0.904
0.4	0.001	0.0	0.999	0.973	0.002	0.892
0.6	0.006	0.0	0.991	0.896	0.018	0.818
0.8	0.021	0.0	0.968	0.576	0.076	0.639

Table 15: TFL, Utility for Suppressing Less Popular Locations/Timeslots (SLP).

z	MRE	MRE 10%	F1	τ	JS	r
0.2	0.001	0.0	1.000	1.000	0.002	0.968
0.4	0.006	0.0	0.999	0.987	0.039	0.891
0.6	0.016	0.0	0.989	0.905	0.149	0.717
0.8	0.031	0.0	0.951	0.797	0.336	0.523

Table 16: SFC, Utility for Suppressing Less Popular Locations/Timeslots (SLP).

w	MRE	MRE 10%	F1	τ	JS	r
0.2	0.010	0.012	0.939	0.222	0.029	0.838
0.4	0.019	0.024	0.905	0.190	0.047	0.759
0.6	0.029	0.036	0.863	0.173	0.068	0.656
0.8	0.038	0.048	0.792	0.160	0.105	0.503

Table 17: TFL, Utility for Sampling (SMP).

w	MRE	MRE 10%	F1	τ	JS	r
0.2	0.011	0.012	0.931	0.329	0.040	0.922
0.4	0.021	0.024	0.894	0.208	0.066	0.849
0.6	0.032	0.036	0.846	0.145	0.099	0.751
0.8	0.042	0.048	0.761	0.099	0.160	0.594

Table 18: SFC, Utility for Sampling (SMP).

k	MRE	MRE 10%	F1	τ	JS	r
2	0.434	0.000	0.829	0.646	0.080	0.570
5	0.439	0.000	0.824	0.584	0.084	0.553
10	0.440	0.001	0.815	0.449	0.085	0.548
20	0.440	0.001	0.801	0.309	0.086	0.546
40	0.439	0.002	0.795	0.201	0.086	0.546
80	0.439	0.002	0.795	0.159	0.086	0.546

Table 19: TFL, Utility for Perturbing Small Counts with $\epsilon'=1.0$ (PSC).

k	MRE	MRE 10%	F1	τ	JS	r
2	3.397	0.000	0.961	0.810	0.163	0.610
5	3.411	0.000	0.949	0.780	0.185	0.567
10	3.427	0.000	0.930	0.749	0.204	0.534
20	3.478	0.000	0.897	0.696	0.228	0.474
40	3.448	0.002	0.840	0.546	0.249	0.417
80	3.417	0.006	0.754	0.217	0.255	0.395
160	3.429	0.009	0.746	0.116	0.255	0.393

Table 20: SFC, Utility for Perturbing Small Counts with $\epsilon'=0.1$ (PSC).

ϵ	MRE	MRE 10%	F1	τ	JS	r
0.01	112.526	0.381	0.124	0.034	0.666	0.005
0.1	11.310	0.058	0.251	0.032	0.412	0.043
1.0	1.149	0.022	0.721	0.043	0.175	0.236
10.0	0.087	0.020	0.758	0.053	0.116	0.447

Table 21: TFL, Utility for Fourier Perturbation Algorithm (FPA).

ϵ	MRE	MRE 10%	F1	τ	JS	r
0.01	74.957	0.106	0.136	0.047	0.577	0.001
0.1	22.855	0.052	0.220	0.008	0.523	0.034
1.0	2.387	0.013	0.784	0.093	0.218	0.263
10.0	0.234	0.011	0.841	0.137	0.107	0.540

Table 22: SFC, Utility for Fourier Perturbation Algorithm (FPA).

w	MRE	MRE 10%	F1	τ	JS	r
0.2	0.444	0.012	0.777	0.091	0.099	0.505
0.4	0.449	0.024	0.741	0.066	0.119	0.448
0.6	0.454	0.036	0.688	0.054	0.150	0.374
0.8	0.460	0.048	0.570	0.042	0.214	0.261

Table 23: TFL, Utility for Sampling & Perturbing Small Counts with $k=5$ and $\epsilon'=1.0$ (SPSC).

w	MRE	MRE 10%	F1	τ	JS	r
0.2	3.348	0.012	0.812	0.248	0.263	0.410
0.4	3.394	0.024	0.698	0.122	0.311	0.333
0.6	3.388	0.036	0.504	0.037	0.379	0.237
0.8	3.459	0.047	0.279	-0.011	0.481	0.115

Table 24: SFC, Utility for Sampling & Perturbing Small Counts with $k=20$ and $\epsilon'=0.1$ (SPSC).

w	MRE	MRE 10%	F1	τ	JS	r
0.2	0.033	0.025	0.757	0.052	0.113	0.452
0.4	0.036	0.033	0.754	0.051	0.115	0.419
0.6	0.040	0.041	0.750	0.051	0.118	0.372
0.8	0.044	0.050	0.736	0.046	0.129	0.290

Table 25: TFL, Utility for Sampling & Fourier Perturbation Algorithm with $\epsilon=10.0$ (SFPA).

w	MRE	MRE 10%	F1	τ	JS	r
0.2	0.214	0.016	0.839	0.137	0.109	0.526
0.4	0.192	0.025	0.838	0.135	0.112	0.506
0.6	0.159	0.036	0.834	0.129	0.119	0.477
0.8	0.109	0.048	0.824	0.111	0.134	0.413

Table 26: SFC, Utility for Sampling & Fourier Perturbation Algorithm with $\epsilon=10.0$ (SFPA).